4.3 W-ALLOY AND COMPOSITE FRACTURE TEST METHOD DEVELOPMENT AND INITIAL EXPLORATION OF DUCTILE PHASE TOUGHENING —

G. R. Odette, E. Stergar[1], D. Gragg, K. Fields, and J. Heathcote[2] (University of California, Santa Barbara), C. H. Henager and R. J. Kurtz (Pacific Northwest National Laboratory)

OBJECTIVES

The objectives of this work include to: a) develop and apply methods to measure the fracture toughness of brittle W and brittle W matrix composites; and b) carry out an initial study of ductile phase toughening in a W-Cu model composite.

SUMMARY

There are many claims in the literature regarding various approaches to *"ductilizing"* W that are difficult to assess, in part because different tests have been used to *"characterize"* the various alloys. Thus one objective of this work is to demonstrate the application of accepted fracture mechanics test methods, so as to provide a common toughness-based metric for comparing different W alloys and composites. A major challenge to testing monolithic W is pre-cracking a very brittle material. A variety of approaches to pre-cracking an elemental W plate were attempted. The most successful method was compression fatigue applied in the axial direction of a small, initially notched bend bar, with the crack in the (T-L) orientation. The linear elastic toughness was measured in 3-point bend tests and averaged K_{Ic} = 8.34±0.43 MPa√m.

A second testing challenge is associated with ductile phase toughened composites. In this case it is necessary to measure the toughness resistance curve associated with extensive stable crack growth. The resistance curve is expressed in terms of J_r/K_r-da curves. Ductile phase toughening (DPT) is largely due to the formation an intact bridging zone behind the tip of crack, which results in a increase in the remote load stress intensity needed for continued crack growth with increasing crack length, da. The main challenge in this case was measuring da as a function of the load (P) and load point displacement (δ). We successfully characterized a K_r-da curve for a W-25%Cu heavy metal composite by combining load P-δ curves with digital image correlation (DIC) measurements of crack growth on the specimen surfaces that could not be observed by normal optical methods. The W-Cu system also served as a model system for an initial exploration of DPT of W composites. The results showed that DPT increased the maximum load toughness of the composite to an average of 24.9±3.5 MPa√m, or a maximum load capacity of ≈ 3 times higher than for monolithic W. The detectible initiation toughness of the composite, marking persistent crack growth, was also increased to ≈ 45 MPa√m compared to 8.34 MPa√m for the monolithic W. More importantly, extensive stable crack growth in the composite provided a major increment of effective post-peak load plastic ductility that is completely absent in linear elastic, monolithic W.

---

[1] Current address SCK Laboratory, Belgium
[2] Current Address Readly College, Readly, CA

PROGRESS AND STATUS

Introduction

This extended background section and associated references were extracted from a successful proposal to OFES entitled *Ductile-Phase Toughened and Fiber-Reinforced Tungsten for Plasma Facing Materials*. This section is included here because we believe that it provides a concise summary of ductile phase toughening of brittle matrix composites, which holds the promise of transforming W to an effective structural material for fusion applications. Tungsten (W) and W-alloys are the leading candidates for the plasma facing components (PFCs) of future fusion power systems because of their high melting point, strength at high temperatures, high thermal conductivity and low sputtering yield [1-5]. In fact, W and W-alloys (hereafter referred to as W-alloys) are almost certainly the material of choice for this extreme service application. However, W-alloys exhibit low fracture toughness and high brittle to ductile transition temperatures (DBTT) that will require them to be treated as fully elastic fracture brittle material in ITER or for DEMO reactor design and operation [1, 3, 6]. The poor starting mechanical properties of W-alloys will be further degraded by radiation damage even at elevated temperatures [7, 8]. The DBTT for unirradiated W-alloys typically ranges from 300 to 400˚C up to ~1000°C, and as noted above, radiation hardening would further elevate the DBTT [3, 9, 10]. Operation of W-alloys at even higher temperatures is limited by re-crystallization of fine grain structures that also degrades toughness [6, 11-13].

Metallurgical approaches to toughen W-alloys, including alloying with Re at concentrations up to 26% [10] and severe plastic deformation (SPD) [14], result in modest to significant toughness increases, and corresponding decreases in the unirradiated DBTT [14]. However, to date, there is no common basis to compare the various W-alloys, since the mechanical characterization methods used to declare an alloy to be “ductilized” have ranged from tensile tests, to smooth bar bend tests [14] to, in only a few cases, actual fracture toughness tests [14]. Thus one objective of this work is to develop and demonstrate a common protocol for testing W-alloys and measuring their fracture toughness.

Ductilizing W is a grand challenge. For example, severe deformation would be very difficult to implement in processing alloys and fabricating structures. Perhaps the most promising toughness increase was observed for the W-26%Re alloy [10]. However, this alloying approach suffers both from high costs and the potential for irradiation-induced precipitation (RIP) of Re-W intermetallic phases, which would produce significant hardening and embrittlement even at low dpa. Transmutation product Re is generated in W and the total concentration when RIP becomes a concern is not precisely known, but is probably less than 10% [15-17]. Claims of significant toughening by fine particle stabilized grains remain largely unproven, in part because of the ambiguous testing methods noted above.

The principles of DPT are illustrated in Figure 1 [18-23]. Figure 1b schematically shows ductile bridging ligaments being stretched in the wake of an open crack in a brittle matrix [22], such as W. A highly effective resistance curve toughening mechanism develops as a crack extends in a brittle matrix containing a suitable volume fraction of the ductile phase. Specifically, as a crack grows in the brittle matrix, it leaves behind a bridging zone of ductile ligaments over a length *L* behind the crack-tip. As cracks continue to

extend, L increases. For small scale bridging (SSB), when the ductile phase bridging zone is much smaller than the crack length, L reaches a steady state length, L_{SSB}. The ligaments produce crack face closure tractions acting in opposition to the applied loading stress intensity factor (SIF), $K_{Applied}$, thus reducing (shielding) the net crack tip SIF, $K_{Tip} < K_{Applied}$. Crack growth occurs when $K_{Tip} = K_{Matrix}$, the toughness of the brittle matrix. The closure stresses are determined by a ductile ligament stress-crack opening displacement function, $\sigma(u)$. The crack opening, u, increases with distance behind the crack-tip, and the reinforcement breaks at a critical u^* where $\sigma(u^*) = 0$ and a maximum L_{SSB} and steady-state K_{SSB}. Thus, an initially un-bridged crack begins to grow when $K_{Applied} = K_{Matrix}$. But as the crack grows L and $K_{Applied}$ needed for $K_{Tip} = K_{Matrix,}$ increase, producing a resistance curve, $K_r(da) > K_{Matrix}$, up to a maximum steady state, K_{SSB} at $da = L = L_{SSB}$. Energy principles can determine K_{SSB}, which depends only on K_{Matrix}, the $\sigma(u)$ work of the ductile phase rupture (in a non-dimensional form, χ) and the elastic modulus (E, see below) [19, 22].

While the concept of DPT is quite simple, the mechanics are more complex [22, 27]. Even for SSB it is necessary to model $K_r(da)$ based on self-consistent solutions for the $\sigma(u)$, $u(L)$ and $\sigma(L)$ functions [22]. Details of $K_r(da)$ are important because, for example, the strength of a composite in the presence of microcracks is primarily determined by the initial $K_r(da)$ slope, while for large cracks, the $K_r(da)$ closer to K_{SSB} controls fracture. Thus it is necessary to know the composite constituent properties from careful analysis and measurements, including for the ductile phases in the composite environment [22, 23, 28].

If DPT occurs under large-scale bridging (LSB) conditions, when L is not very small compared to the crack length, the entire $K_r(da)$ resistance curve behavior depends in a complicated way on the length scales and geometries of the reinforcement and the cracked body. In this case, as Figure 2a shows, very large increases in K_r are possible [22]. Application to composite structures requires that the $K_r(da)$ information be converted to remote applied load (P) and load-displacement (δ) functions, $P(\delta)$, for the cracked body. Figure 2b shows that $K_r(da)$ can be modeled based on the $\sigma(u)$, E and K_{Matrix} properties that can be both independently measured and modeled (see below). Figure 2c shows that DPT provides composite ductility as well as large strengthening factors compared to the brittle matrix. The most important composite constituent property is the $\sigma(u)$ function, which also depends in a complicated way on both intrinsic material properties of the ductile phase and extrinsic factors such as the reinforcement size, geometry, and other effects such as de-bonding from the brittle matrix. Thus the mechanics controlling $\sigma(u)$ is critical, and must be modeled using finite element methods [29, 30]. The most important take away point is that this complexity is a real advantage because: 1) it can be modeled and analyzed to predict the behavior of a structure; and 2) the variety of mechanisms and mechanics can be used to tailor and optimize DPT composite design for particular applications. It is our opinion that purely empirical efforts to develop W-composites that are not guided by proper understanding of the mechanisms and mechanics are likely to be expensive failures.

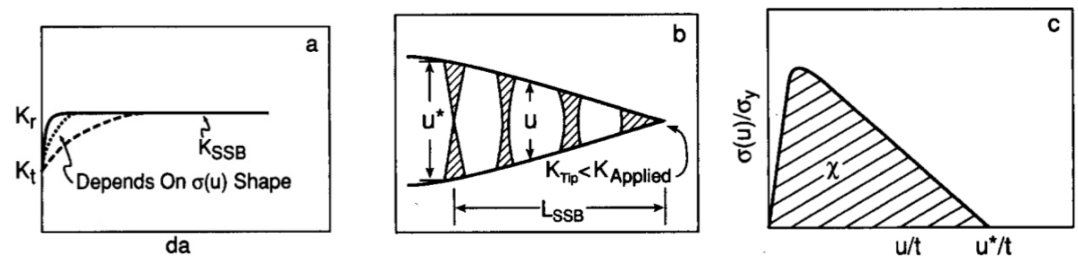

(a) (b) (c)

Figure 1. Schematic representation of ductile phase toughening: (a) Crack growth resistance curve behavior and steady-state toughness; (b) a steady-state bridge zone shown schematically in 2D; and (c) a typical normalized stress-displacement function and work of rupture, *c* for a DPT composite [22]. Symbols and terms are defined in the text above.

It is useful to provide more detail on one specific example of a DPT composite shown in Figure 2, Odette et al. fabricated a γ-TiAl/TiNb laminate by hot pressing and forging TiNb foils with TiAl powders to produce 105-μm layers of TiNb separated by about 500-μm of γ-TiAl matrix plus a thin α_2 reaction layer [22]. Chevron-notched three point bend specimens were machined from the starting material, which contained about 22% TiNb as the ductile phase reinforcement. Crack growth resistance curve, $K_r(da)$, tests were carried out under displacement control as a function of incremental crack length. The results were compared to the predicted SSB DPT toughening. For SSB the maximum net K_{SSB} is given by

$$K_{SSB} = \left(K_{\chi}^{2} + K_{Matrix}^{2}\right)^{1/2}$$
$$K_{\chi} = \left(E\,\sigma_y t f \chi\right)^{1/2} \qquad (1)$$
$$\chi = f \int_0^{u^*} \left(\frac{\sigma(u)}{\sigma_y}\right) \frac{du}{t}$$

The $\sigma(u)$ is the absolute ductile phase ligament stress-displacement function. The non-dimensional χ is defined in terms of the corresponding crack face ductile phase area fraction (f), ligament thickness (t), yield stress (σ_y), and rupture displacement (u^*). Here E is the composite elastic modulus needed to relate K to the corresponding plastic work (J) as $K = [EJ]^{1/2}$. Normally K_c is much greater than K_{Matrix}, so the former has the dominant effect on the toughness, while the latter, along with E, has relatively less effect. Thus, from the perspective of gross mechanical failure, even if matrix toughness is low and further degraded in service by radiation damage, the consequence to composite behavior is greatly mitigated. Further, as discussed below, under LSB, when the bridging zone is not small compared to crack dimensions, the composite toughness is much greater than for SSB.

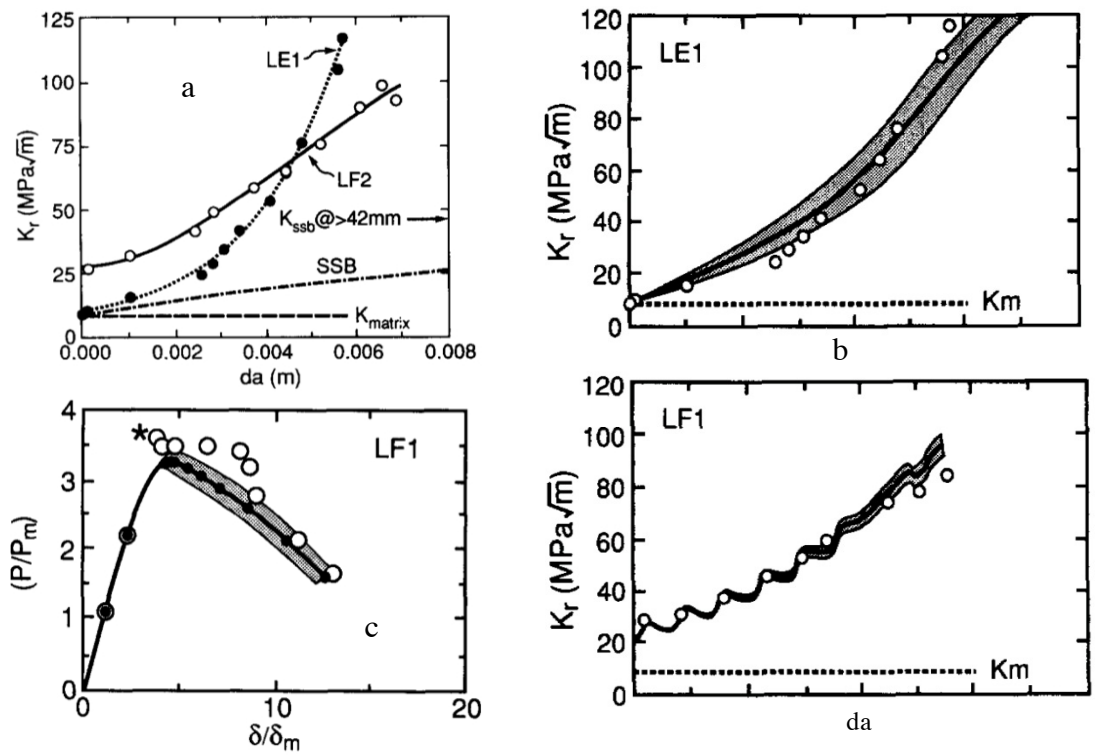

Figure 2. (a) Crack growth resistance curves in the LSB regime for a TiAl-TiNb composite showing large increases in toughness; (b) the corresponding normalized predicted and measured $K_r(da)$ curves showing enormous increases in toughness; and c) a corresponding $P(\delta)$ curve showing both large strengthening (≈ x3.5) and ductility increases (≥ x13) provided by DPT [22].

In the previous research of Odette and co-workers [22], the $\sigma(u)$ function was independently measured under constrained deformation conditions using sandwich TiAl/TiNb/TiAl specimens containing pre-cracks [31]. These independent measurements are critical since residual stresses and constraints affect the $\sigma(u)$ function relative to tensile test measurements. Rigorous modeling of LSB was carried out based on the independent $\sigma(u)$ function by calculating self-consistent solutions for the crack opening profile $u(x)$ and the corresponding crack face distribution $\sigma(x)$, where x is the distance from the crack tip, for a specified set of $\sigma(u)$, E, and K_{tip} composite properties [22]. Figure 2b shows the resistance curves from the model (lines) and the experimental measurements (symbols), for edge and face (E and F) orientations, where the crack intersects the edges and faces of the ductile layers, respectively. Figure 2a shows that: i) enormous DPT occurs under LSB that greatly exceeds that found for either the monolithic TiAl (which has a K_{Ic} similar to that of W at room temperature) and SSB conditions; ii) the F orientation initially provides an extra increment of K_r since cracks arrested at one face of a ductile layer must be re-nucleated on the back face to continue propagating; iii) the model is in good agreement with experiment; iv) extensive stable crack growth occurs for the LSB conditions; and v) the corresponding slope of the resistance, dK_r/da, curve is low. Figure 2c shows the benefits of DPT on the effective composite strength and ductility. Here, the P-δ curves (that are akin to the engineering

stress and strain curves) have been normalized by the corresponding fracture loads and displacements of the brittle matrix (subscript m). Again the model predictions are in good agreement with experimental measurements. The load and displacement capacity of the composite exceeds that of the matrix by factors of more than 3 and 10, respectively. The results indicate that: i) DPT under LSB conditions can produce enormous increases in resistance curve toughness; ii) resistance curve toughening can be rigorously modeled in terms of the properties of the composite constituents; and iii) the toughening can be modified by choices in the reinforcement material and architecture. The models can also be used to assess component failure limits including the effects of compliance.

For example, if the objective is to increase the strength of a composite in the presence of micro-cracks, then micron scale reinforcements (much smaller t) are better, since the initial slope of the $K_r\ (da)$ curve is larger in this case [32-37]. The DPT principles and models described above are also applicable to measuring and modeling enhanced composite strength and ductility. Indeed, a general design approach to optimizing the composite architecture tailored to a specific application has been developed based on the SSB and LSB bridging mechanics combined with finite element method (FEM) models of $\sigma(u)$ functions and the various factors that individually and in combination control them [32, 34, 36, 37].

Heathcote and Odette have used combinations of SSB/LSB and FE $\sigma(u)$ models to develop a set of quantitative design tools that permit the optimization of a DPT composite strength for a particular application [32-34, 36, 37]. An example is shown in Figure 3a as a map of the strengthening for a specified combination of crack length and ductile layer thickness in both non-dimensional and absolute values for LSB conditions for a baseline $\sigma(u)$ function. The dashed line shows the optimal layer thickness. Similar maps are available for different $\sigma(u)$ functions. Figure 3b shows the effect of layer thickness on the composite strength as a function of layer thickness for the base function and two variants related to internal stresses and constraint loss due to de-bonding for a 40-µm microcrack. The increases in peak strength correspond to increases in the slope of the initial $K_r(da)$ resistance curve. This work also developed a method to derive critical composite $\sigma(u)$ curves directly from $K_r(da)$ resistance curves and confocal microscopy-fracture reconstruction (CM-FR) characterization of the three dimensional topology of ruptured or fractured ductile ligaments [32-34, 36, 37]. In addition to the macro- and micro-laminates, research of Odette and co-workers also includes composites reinforced with discrete ductile phase particles [23, 38-40].

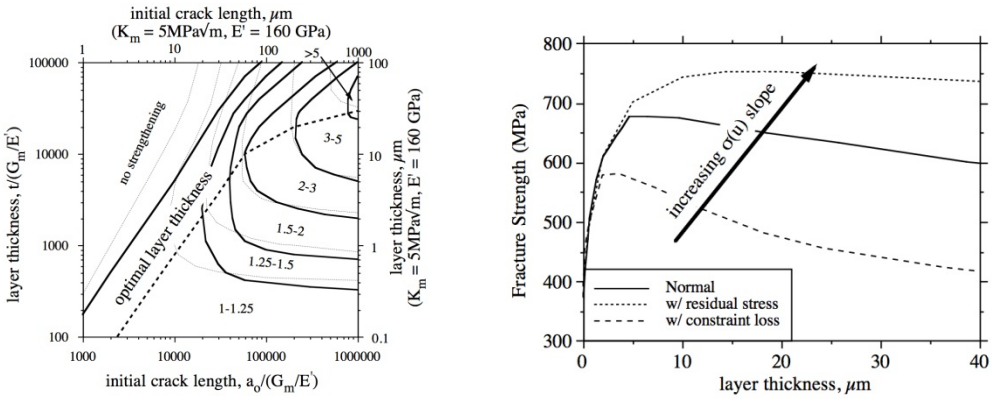

Figure 3. (a) A strength map showing the effect of constraint loss (curves for fully constrained deformation are shown as dashed lines for reference). The various solid curves correspond to ranges of strengthening ratios. The curve for the optimal layer thickness for strengthening is shown as the dashed line. (b) Fracture strength as a function of layer thickness for a composite with a plane strain elastic modulus of 160 GPa, a matrix toughness, G_m, of 100 J/m^2 (K_m = 4 MPa√m), and an initial crack size of 40 μm. Increasing the slope of the *σ(u)* curve (through either deformation constraint or residual stresses) causes an increase in the strength for layer thicknesses above a few microns, especially at the optimal layer thickness, and decreases the sensitivity of the fracture strength on the layer thickness for 10 < *t* < 40 μm.

Several other issues that have been addressed in previous work, but that will require additional study, include the role and mechanics of de-bonding [33, 34, 36, 37, 41, 42], composite behavior under fatigue loading conditions [23, 38, 43] and dynamic (high rate) loading conditions [43]. However, the examples shown here clearly demonstrate that there is a rigorous quantitative scientific foundation of experimental methods and analysis to design and test DPT W-composites that are optimized for plasma facing component service.

Experimental Methods

A 4.0 mm thick plate of unalloyed W, initially produced by Plansee, was obtained from Michael Reith at KIT. The W was fabricated by de-oxidizing and then HIPing powders to nearly full consolidation. The resulting consolidated W was then rolled to the plate thickness. Further details on the material and processing path will be supplied elsewhere. But it is sufficient here to say that this unalloyed, monolithic W can be considered a baseline *"garden variety"* material for comparison to other W alloys and composites.

Fracture tests were carried out on 3.2mm x 1.575mm x 18mm bend bars. To date testing has been confined to the T-L orientation as shown in Figure 4a, with the crack propagating in the rolling direction; T-L is generally considered to be the most brittle orientation. Two bars were EDM notched to a depth (a_n) over width (W) ratio of a_n/W = 0.3 and four bars were EDM notched to a depth (a_n) over width (W) ratio of a_n/W = 0.5.

The bars were then pre-cracked by cyclic axial compression loading as illustrated schematically in Figure 4b [44]. Sharp pre-cracks were then grown from the notch to a small increment of extension with a typical pre-crack extension of ≈ 0.4 mm for the specimens with a_n/W = 0.3 and pre-crack extension of ≈ 0.135 mm for the specimens with a_n/W = 0.5. Six pre-cracked specimens were then tested at ambient temperature in three-point bending on a hydraulic load frame at a displacement rate of 0.1 mm/min. All fractures were linear elastic, and the K_{Ic} were evaluated based on the ASTM E399 test method [45].

The W-25wt%Cu heavy metal composite, Copelmet ®, was purchased from Goodfellow Co in the form of a rectangular bar with a 25mm x 25mm cross section. Although Goodfellow does not specify hoe the material is manufactured, we believe that the composite bar was initially processed by the standard route by making a porous pre-form out of the W-powders that was then pressure infiltrated with molten Cu and sintered. The volume fraction of Cu is about 50%. Hardness, SEM fractography and confocal microscopy-fracture reconstruction measurements were carried out as well as fracture testing. Further details of the material, processing path and experimental methods will be provided elsewhere.

The small bend bar specimens used for the composite were the same as those for the monolithic W testing and were fabricated from the bar as illustrated in Figure 4c. The bend bars were also notched and fatigue pre-cracked in 3-point bending. The subsequent resistance curve tests were also carried in 3-point bending, in some cases with unloading cycles. A resistance K_r-da curve is characterized by an initiation K_{Ic} marking the nominal onset of crack extension (da) followed by an increasing K_r(da) with increasing crack length, a. In order to determine K_r(da), the da must be combined with the P-d curve to determine increments of DK_r with da. Note this can be done either using the J-integral method [46] or computing the nominal stress intensity factor K_I for the remote loads and instantaneous crack length, a_o + da. The resistance curve da is typically measured by unloading compliance or, in some cases, electro-potential drop methods. However, these techniques do not work in cases where there is a bridging zone behind the crack tip. It is sometimes possible to optically measure da on the specimen surface; and this approach is reasonably valid for brittle matrix composites. However, the surface of the W-Cu composite is too complex (mottled and irregular) and cannot be sufficiently polished to permit accurate measurements of the da for fine cracks. Thus we used a digital image correlation (DIC) method instead. DIC provides a very high-resolution map of 2-D (in this case) displacement fields by comparing the sequential positions of small surface features over an increment of loading, or in this case, crack extension. The displacement fields can also be converted to strain fields. The fields can readily show crack the extension, da, on painted (white) and speckled (black) surface. An example is shown in Figure 5.

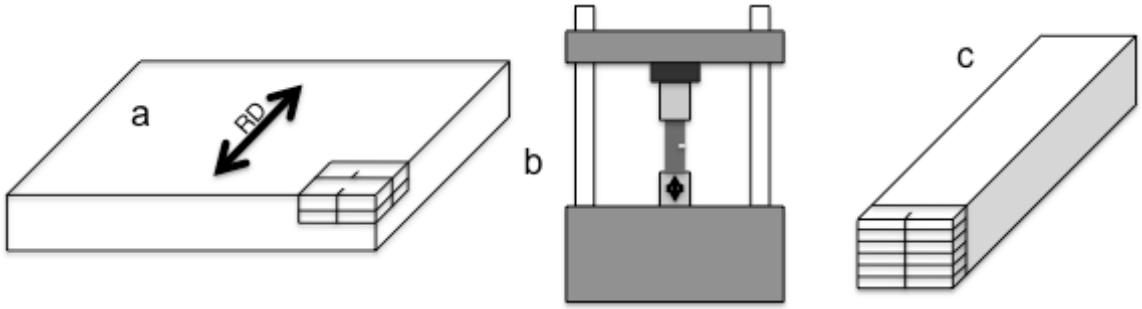

Figure 4. a) T-L orientation of the fracture specimens in the W plate; b) schematic of the compression fatigue method or unalloyed W; c) layout of the fracture specimens in the W-Cu compsite.

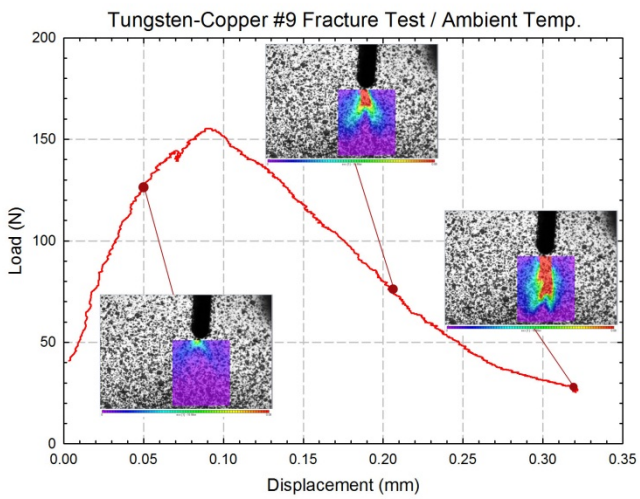

Figure 5. A typical load displacement curve for the W-composite and the corresponding assessment of the crack extension, da, using the DIC method.

Table 2 summarizes the K_{Ic} data for the monolithic W plate. The Vickers microhardness of the composite was measured at 204 kg/mm^2.

Figure 6 compares the P-δ curves for the monolithic W plate and the W-Cu composite for specimens with the same a_o/W. The increase in the maximum P and much larger δ are clear. The average maximum load K_{Jcm} for 8 tests is 24.9 MPa√m ≈ 3 times and the average δ_c ≈ 7.5 times the K_{Ic} and δ_c for the monolithic W. The P versus a curve measured by the DIC method is shown in Figure 7. There is some chatter in near da ≈ 0 that is likely associated with cracking before actual propagation begins, and P decreases approximately linearly with da after that. Figure 8 shows the corresponding J_r-da curve where the equivalent K_r is given by √JE' where E' is the effective plain strain elastic

modulus of the composite taken as E' = xxx GPa. This data suggest that the initiation toughness is ≈ 45 MPa√m and the maximum K_r in the test is ≈ 75 MPa m.

Table 2. Summary of the K_{Ic} measured in the W Plate

K_{Ic} MPA√m
7.8
8.35
8.99
8.6
7.8
8.35

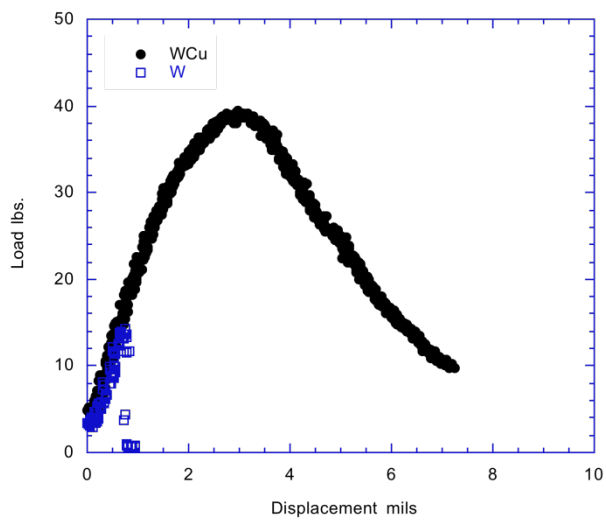

Figure 6. A typical load-displacement curve for the linear elastic W plate and the W-Cu composite manifesting extensive stable crack growth and resistance curve behavior.

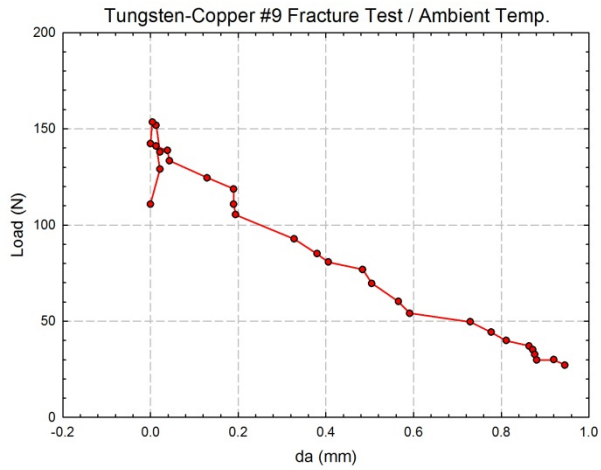

Figure 7. Load versus crack extension in the W-Cu composite measured by the DIC method.

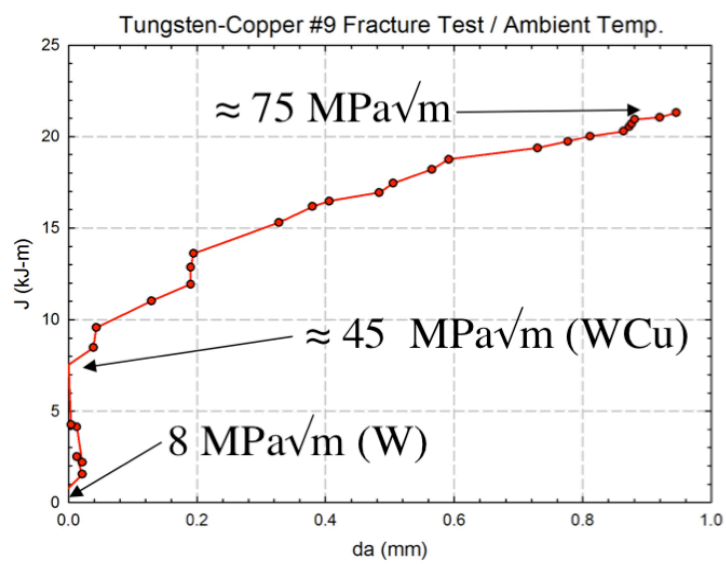

Figure 8. A J_r-da resistance curve for the W-Cu composite.

Figure 9 shows facture surface of the composite with a mixture of brittle cleavage in W and ductile ligament fracture in the Cu. Figure 10 shows a confocal microscopy-fracture reconstruction (CM-FR) 3D map of a region of the fracture surface. These techniques, and others, will be used to develop a fully quantitative model of DPT in the W-Cu system that will serve as a template for future research on developing W-composite based divertor components.

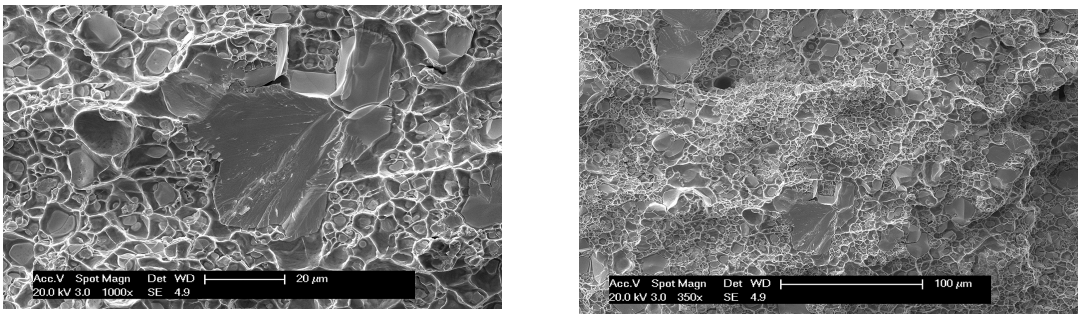

Figure 9. The fracture surface of the W-Cu composite showing a mixture of cleavage (W) and ductile fracture (Cu).

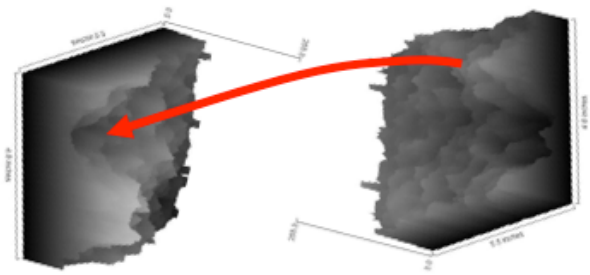

Figure 10. CM-FR images of conjugate fracture surfaces in the W-Cu composite sowing the ductile behavior of the Cu reinforcement phase.

SUMMARY AND FUTURE WORK

A reasonable value for the room temperature toughness of unalloyed rolled W plate in the T-L orientation is $K_{Ic} \approx 8$ MPa√m. Thus similar tests on so-called ductilized W will be needed to compare to this benchmark value. Efforts will continue to develop mechanical testing protocols for W alloys (and composites), including improved pre-cracking methods and extension of the measurements to high temperature. These test methods will be applied to improved W-alloys and composites as they become available.

An exploratory study of a model W-composite yielded very encouraging results. A commercial W-25%Cu heavy metal composite showed a much a higher effective toughness compared to the monolithic plate. The improved fracture resistance is manifested by a higher initiation toughness followed and extensive stable crack growth that is controlled by a significant resistance K_r-da curve. The much higher composite toughness is due to DPT associated with LSB mechanics. The composite has an approximately 3 times higher maximum load capacity compared to the W plate and more that 7 times the deflection capacity that is akin to plastic ductility. Future work on the W-Cu composite will focus on extracting the critical ductile phase constituent σ(u) function

based on a combination of 3-D fractography (CM-FR), inverse LSB modeling of the test observables and finite element simulations. This work is providing an important foundation for a new initiative that UCSB will be undertaking in collaboration with PNNL to develop structural W composites.

REFERENCES

1. M. Rieth, J. L. Boutard, S. L. Dudarev, et al., *J. Nucl. Mater.* **417** (2011) 463.
2. R. A. Pitts, A. Kukushkin, A. Loarte, et al., *Phys. Scrip.* **T138** (2009) 014001.
3. P. Mertens, T. Hirai, M. Knaup, et al., *Fus. Eng. Design* **84** (2009) 1289.
4. A. Gervash, R. Giniyatulin, T. Ihli, et al., *J. Nucl. Mater. B* (2007) 1472.
5. M. Merola, W. Danner, M. Pick, *Fus. Eng. Design* (2005) 325.
6. P. Mertens, V. Philipps, G. Pintsuk, et al., *Phys. Scrip.* **T138** (2009) 014032.
7. A. Moslang, E. Diegele, M. Klimiankou, et al., *Nucl. Fus.* **45** (2005) 649.
8. M. A. Abdou, A. Ying, N. Morley, et al., *Fus. Eng. Design* **54** (2001) 181.
9. S. J. Zinkle, N. M. Ghoniem, *Fus. Eng. Design* **51** (2000) 55.
10. B. Gludovatz, S. Wurster, A. Hoffmann, et al., *Int. J. Refrac. Met.* **28** (2010) 674.
11. S. Wurster, B. Gludovatz, R. Pippan, *Int. J. Refrac. Met.* **28** (2010) 692.
12. Z. Zhangjian, L. Jochen, G. Pintsuk, et al., *J. Nucl. Mater.* (2009) 733.
13. T. Tanabe, V. Philipps, K. Nakamura, et al., *J. Nucl. Mater.* (1997) 1164.
14. M. Faleschini, H. Kreuzer, D. Kiener, et al., *J. Nucl. Mater.* (2007) 800.
15. T. Tanno, A. Hasegawa, J. C. He, et al., *J. Nucl. Mater.* (2009) 218.
16. T. Tanno, A. Hasegawa, M. Fujiwara, et al., *Mater. Trans.* **49** (2008) 2259.
17. T. Tanno, A. Hasegawa, H. Jian-Chao, et al., *Mater. Trans.* **48** (2007) 2399.
18. V. D. Krstic, M. Komac, *Phil. Mag. A* **51** (1985) 191.
19. A. G. Evans, *Mater. Sci. Eng. A* **105** (1988) 65.
20. L. S. Sigl, P. A. Mataga, B. J. Dalgleish, et al., *Acta Metall.* **36** (1988) 945.
21. T. C. Lu, A. G. Evans, R. J. Hecht, et al., *Acta Metall. Mater.* **39** (1991) 1853.
22. G. R. Odette, B. L. Chao, J. W. Sheckherd, et al., *Acta Metall. Mater.* **40** (1992) 2381.
23. K. T. Venkateswara Rao, G. R. Odette, R. O. Ritchie, *Acta Metall. Mater.* **42** (1994) 893.
24. R. J. Zhang, Y. Q. Yang, W. T. Shen, et al., *J. Cryst. Grow.* **313** (2010) 56.
25. R. J. Zhang, Y. Q. Yang, W. T. Shen, et al., *Thin Solid Films* **519** (2010) 1367.
26. C. Guo, C. Zhang, L. He, et al., *J. Mater. Sci. Technol.* 23 (2007) 677.
27. A. G. Evans, F. W. Zok, *Solid State Phys.* **47** (1994) 177.
28. D. M. Shah, D. L. Anton, D. P. Pope, et al., *Mater. Sci. Eng.* **A192** (1995) 658.
29. L. S. Sigl, S. Schmauder, *Inter. J. Fract.* **36** (1988) 305.
30. H. F. Fischmeister, S. Schmauder, L. S. Sigl, *Mater. Sci. Eng.* ***A105*** (1988) 305.
31. H. C. Cao, B. J. Dalgleish, H. E. Deve, et al., *Acta Met.* **37** (1989) 2969.
32. J. R. Heathcote, University of California, Santa Barbara (1996).
33. J. Heathcote, G. R. Odette, G. E. Lucas, et al., *Acta Mater.* **44** (1996) 4289.
34. J. Heathcote, G. R. Odette, G. E. Lucas. Symposium, (1996) PA, USA: *Mater. Res. Soc.*
35. R. G. Rowe, D. W. Skelly, M. Larsen, et al., *Scr. Metall. Mater.* **31** (1994) 1487.
36. J. A. Heathcote, G. R. Odette, to be published.
37. J. A. Heathcote, G. R. Odette, to be published.
38. K. T. Venkateswara, G. R. Odette, R. O. Ritchie, *Acta Metall. Mater.* **40** (1992) 353.
39. G. R. Odette, H. E. Dève, C. K. Elliott, et al., Symposium (1990) TMS.
40. C. K. Elliott, G. R. Odette, G. E. Lucas, et al., *Mater. Res. Soc.* (1988). Boston, MA: MRS.

41. H. E. Deve, A. G. Evans, G. R. Odette, et al., *Acta Metall. Mater.* **38** (1990) 1491.
42. J. A. Heathcote, G. R. Odette, G. E. Lucas, et al., Symposium (1996) MRS.
43. J. A. Heathcote, G. R. Odette, to be published.
44. R. Pippan, *Fatigue Fract. Eng. Mater. Struct.* **9** (1987) 319.
45. Standard Test Method for Linear-Elastic Plane-Strain Fracture Toughness K_{Ic} of Metallic Materials, ASTM E399 - 09E2, ASTM Book of Standards 3.01 (2011).
46. Standard Test Method for Measuring Fracture Toughness, ASTM E1820-08, ASTM Book of Standards 3.01 (2011).